Convolutional Neural Network Optimize the Application of Diffusion Kurtosis Imaging in Parkinson's Disease

Junyan Sun
Department of Neurobiology, Neurology and Geriatrics, Xuanwu Hospital of Capital Medical University, Beijing Institute of Geriatrics,Beijing, China https://orcid.org/0000-0002-2524-6133

Ruike Chen
Center for Brain Imaging Science and Technology, College of Biomedical Engineering and Instrumental Science, Zhejiang University, Hangzhou, Zhejiang,China. 310027

Qiqi Tong
Research Center for Healthcare Data Science, Zhejiang Lab, Hangzhou, Zhejiang,China

Jinghong Ma
Department of Neurology, Xuanwu Hospital of Capital Medical University,Beijing,China

Linlin Gao
Deparment of Neurology, Neurology and Geriatics, Xuanwu Hospital of Capital Medical University, Beijing Institute of Geriatrics, Beijing, China

Jiliang Fang
Department of Radiology, Guang'anmen Hospital, China Academy of Chinese Medical Sciences, Beijing,China

Dongling Zhang
Department of Neurology, Neurology and Geriatrics, Xuanwu Hospital of Capital Medical University, Beijing Institute of Geriatrics, Beijing, China

Piu Chan
Department of Neurobiology, Neurology and Geriatrics, Xuanwu Hospital of Capital Medical University, Beijing Institute of Geriatrics, Beijing, China

Hongjian He
Center for Brain Imaging Science and Technology, College of Biomedical Engineering and Instrumental Science, Zhejiang University, Hangzhou, Zhejiang, China. 310027

Tao Wu (wutao69@gmail.com)
Department of Neurobiology, Neurology and Geriatrics Xuanwu Hospital of Capital Medical University

Research

Keywords: parkinson's disease, diffusion kurtosis imaging, convolutional neural network, mean kurtosis, kurtosis fractional anisotropy, mean diffusivity

Posted Date: March 31st, 2021

DOI: https://doi.org/10.21203/rs.3.rs-339908/v1

Abstract

Objectives: This work attempted to assess the feasibility of deep-learning based method in detecting the alterations of diffusion kurtosis measurements associated with Parkinson's disease (PD).

Methods: A group of 68 PD patients and 77 healthy controls (HCs) were scanned on the scanner-A (3T Skyra) (DATASET-1). Meanwhile, an additional 5 healthy travelling volunteers were scanned with both the scanner-A and an additional scanner-B (3T Prisma) (DATASET-2). Diffusion kurtosis imaging (DKI) of DATASET-2 has an extra *b* shell than that of DATASET-1. In addition, a 3D convolutional neural network (CNN) was trained from Dataset 2 to harmonize the quality of scalar measures of scanner-A to a similar level of scanner-B. Whole-brain unpaired t-test and Tract-Based Spatial Statistics (TBSS) was performed to validate the differences between PD and control groups with model fitting method and CNN method respectively. We further clarified the correlation between clinical assessments and DKI results.

Results: In the left substantia nigra (SN), an increase of mean diffusivity (MD) was found in PD group. In the right SN, fractional anisotropy (FA) and mean kurtosis (MK) values were negatively correlated with Hoehn & Yahr (H&Y) scales. In the putamen, FA values was positively correlated with H&Y scales. It is worth noting that, these findings were only observed with the deep-learning method. There was neither group difference, nor correlation with clinical assessments in the SN or striatum exceeding the significant level by using the conventional model fitting method.

Conclusions: CNN method improves the robustness of DKI and can help to explore PD-associated imaging features.

1. Introduction

Parkinson's disease (PD) is a common neurodegenerative disease characterized by bradykinesia, resting tremor, rigidity, posture balance disturbance and non-motor manifestations [1]. Beyond the deficiency of dopaminergic neurons and aggregation of Lewy bodies in the basal ganglia, pathological changes of PD are associated with axonal lesions and synaptic dysfunction, which contributes to the impairments of white matter integrity [2]. Given the limitation of discerning the intrinsic details and pathological heterogeneity in brain tissues, conventional magnetic resonance imaging (MRI) has difficulty in revealing PD-associated microstructural changes. Diffusion-weighted MRI techniques like diffusion tensor imaging (DTI), can non-invasively probe the microstructural properties via the diffusion of water molecules *in vivo* [3–7]. It has been reported that DTI-derived metrics, such as fractional anisotropy (FA) and mean diffusivity (MD), showed significant differences in the substantia nigra (SN) and some white matter areas in PD patients [8]. Further, diffusion kurtosis imaging (DKI), which developed based on DTI and taken the non-Gaussian diffusion of water molecules into account, was reported as a more sensitive technique to evaluate the pathological characteristics of PD patients [5, 8].

However, previous studies yielded inconsistent or even controversial findings. For example, while some studies showed decreased FA value, increased MD and/or mean kurtosis (MK) values in the SN [6, 9–11], other studies [6, 12] observed increased FA value in the SN in PD patients. It has been reported that the FA value of SN in PD patients had a rising tendency compared with healthy controls (HCs) [11]. Additionally, Kamagata et al. found decreased MK and FA values of white matter, such as inferior fronto-occipital fasciculus, anterior corona radiata and superior longitudinal fasciculi [7], while Wen et al. showed increased FA values of inferior fronto-occipital fasciculus and bilateral superior longitudinal fasciculi in tremor dominant PD patients [13].

It is speculated that the heterogeneity of PD patients being recruited and various acquisition protocols of diffusion MRI scanning may contribute to those controversial findings [3, 4, 8, 14]. DKI can sensitively reflect microstructural complexity, particularly in isotropic tissues such as gray matter [15]. But since gray matter microstructure lacks evident directionality, DWI signals can be easily affected by noise and limited spatial resolution [16], thus leading to inaccurate findings of alterations in DKI scalar measures.

Recently, deep learning, an important branch of machine learning, shows noteworthy potential for improving the detection of neuroimaging findings [17–21]. As one of the representative algorithms of deep learning, convolutional neural network (CNN) adopts convolution and down sampling to certain layers with less computation, adjusts the network weights through the back-propagation and stochastic gradient descent algorithm, recognizes the features or patterns of the raw imaging inputs automatically, and then achieves the classification, identification and prediction of inputs [19, 21, 22].

Li et al. [23] recently proposed a three-dimensional hierarchical convolutional neural network (3D H-CNN) to improve the estimation of DKI scalar measures from limited diffusion-weighted images (DWIs). Three-dimensional convolution kernels were introduced to extract and learn features of the DWIs automatically. Only part scalar measures were of clinical interest instead of the full tensors, 3D H-CNN (herein after called CNN) method makes it possible to complete fast and optimize DKI acquisition within 1 minute. It also took the cross-voxel information into account, which was proved to provide enhanced efficiency of estimating DKI scalar measures and improved robustness against noise.

Therefore, in the current study, we aimed to use this CNN method to improve the estimation of DKI scalar measures, and to examine whether the improved measures can help reveal PD-associated imaging features.

2. Materials And Methods

2.1. subjects

Sixty-eight PD patients meeting the Movement Disorder Society clinical diagnostic criteria for Parkinson's disease were recruited from the Movement Disorders Clinic of the Xuanwu Hospital of Capital Medical University. We recruited seventy-seven HCs meeting the following criteria: (1) over the age of 40, (2) no

history of neurological or psychiatric diseases, (3) no family history of neurodegenerative disorders, and (4) no obvious cerebral lesions on structural MRI. The Movement Disorder Society Unified Parkinson's Disease Rating Scale, part III (MDS- UPDRS Ⅲ) and Hoehn & Yahr (H&Y) scale were assessed in all PD patients while they were at off-state. Their demographic details are summarized in Table 1. In addition, five healthy traveling subjects (M/F = 1/4, age = 26.6 ± 1.9 years) were recruited and their DKI data were collected on two different MRI scanners. This experiment was guided by and adhered to the Declaration of Helsinki and was approved by the Institutional Review Board of Xuanwu Hospital. All included participants have signed informed consent before the experiment.

Table 1
Demographic and clinical assessments of subjects.

	PD (n = 68)	HC (n = 77)	p value
age in years, mean (SD)	58.94(8.969)	59.58(8.537)	0.659
gender(M/F) §	36/32	30/47	0.092
H&Y score, median(range)	2(1–3)	0	NA
UPDRS Ⅲ, mean (SD)	26.5(12.261)	NA	NA
duration in years, median(range)	4(0.5–20)	NA	NA
M, male; F, female; SD, standard variation; NA, not applicable.§Pearson's chi-square test			

2.2. MR imaging acquisition

2.2.1. DATASET 1

For all PD patients and healthy controls, MRI data were acquired at a 3T scanner-A (MAGNETOM Skyra, Siemens, Germany) equipped with a 20-channel receiver head and neck joint coil (opening 16 channels). DWIs were obtained axial orientation with single shot spin-echo echo planar imaging sequences (SE-EPI). Diffusion weightings of b = 1000 and 2000 s/mm² were applied along 30 noncollinear sensitive gradients directions. One b = 0 image is acquired, resulting a total of 61 DWIs. Other imaging parameters were as follow: repetition time (TR) = 5000 ms, echo time (TE) = 105 ms, resolution = 2mm×2mm×2mm, field of view (FOV) = 220mm×220 mm, number of slices = 68.

2.2.2. DATASET 2

Five travelling subjects were scanned on two different MRI scanners. Scan 1 was also using the scanner-A and same scanning process as performed in the DATASET 1. For implementation of CNN, DWIs were also acquired in the Scan 2 using a 3T scanner-B (MAGNETOM Prisma, Siemens Germany) equipped with a 64-channel RF coil. The DWIs were obtained using a simultaneous multi-slice diffusion echo planar imaging sequence (SMS-EPI). Diffusion weightings of b = 1000, 2000 and 3000 s/mm² were applied in 30 gradient directions. Six b = 0 images and one b = 0 image with an opposite phase encoding direction were

acquired,resulting in a total of 96 DWIs. The one $b = 0$ image with reversed phase encoding direction was for correcting the field inhomogeneity-induced distortion. Other imaging parameters were as follow: repetition time (TR) = 3000 ms, echo time (TE) = 75 ms, resolution = 2mm×2mm×2mm, FOV = 220mm×220 mm, number of slices = 68.

2.3. Image processing

2.3.1. preprocessing

The preprocessing pipeline for both datasets was mainly based on FSL (FMRIB Software Library, University of Oxford, UK) [24]. *Rician* noise was removed using *dwidenoise* included in MRtrix 3 [25], followed by gibbs-ring removal. For DATASET 2, Scan 2, distortion correction was also performed using *topup* and *eddy* tool [26]. The susceptibility-induced off-resonance field map was first estimated by *topup* using a pair of non-DW ($b = 0$) images acquired with reversed phase encoding directions AP and PA. It was then fed into *eddy* to perform correction for eddy current and motion induced distortion.

2.3.2. model fit

For the DATASET 1 and Scan 2 of DATASET 2, model fitting method was conducted using DESIGNER (Diffusion parameter EStImation with Gibbs and NoisE Removal, New York University, US), which is a post-processing pipeline capable of identifying and correcting various specific artifacts and confounding factors for an improved accuracy, precision, and robustness compared to traditional linear least square method fitting (Figure. 1) [27].

2.3.3. CNN

CNN method was adopted to improve the estimation of DKI scalar measures from limited quality of DATASET 1. The adopted CNN method included one input layer, several hidden layers and two output layers. A dropout layer was inserted before each output layer to prevent overfitting. 3×3×3 convolution kernels were introduced in the first hidden layer to extract features from the preprocessed DWIs. The network was constructed in a hierarchical structure. Resulting DKI scalar measures were output through two different layers. The shallow output layer was connected to the penultimate hidden layer and was responsible for the scalar measures (FA and MD). Kurtosis related measures (MK and KFA) values were output through a deeper layer connected to the last hidden layer [23].

Preprocessed DWIs of DATASET 2, Scan 1 were the training data of CNN and the corresponding model-fitted MK, KFA, FA, and MD maps for each traveling subject in DATASET 2, Scan 2 were defined as training and test labels. Scan 2 were registered to Scan 1 using non-linear registration before training. Preprocessed DWIs of DATASET 1 were used as test sets (Figure. 1).

The entire training and testing pipeline of CNN is as displayed in Fig. 2. Preprocessed DWIs of Scan 1 and the reference standard DKI maps derived from scan 2 were input as the training and labeling datasets in the training phase. Noise and gibbs-ring removed DWIs of DATASET 1 were the inputs as the testing

phase. DWIs of Scan 2 included higher *b* values and more diffusion weighted directions than Scan 1. The additional $b = 0$ images with reversed phase encoding directions allows correction for field inhomogeneity induced distortion. All improvements in scanning condition resulted in a better quality of DWIs and a better estimation of DKI scalar measures compared with model fitting method. The CNN training process related limited quality DWIs with its corresponding high-accuracy DKI scalar measures, gaining the network an ability to predict high-quality DKIs from moderate DWIs (Figure. 1). As shown in Figure. 1 and Figure. 2, DKI scalar maps estimated by CNN of both dataset 1 and 2 had higher signal-to-noise ratio (SNR) than those by model fitting. For dataset 2 the CNN results displayed almost equivalent quality as the reference standard (ground truth).

2.4. Statistical analysis

The 1-sample Shapiro-Wilk test was applied to confirm the normality of each group data. The Student's *t* test and Pearson chi-square test were used for age and sex variables, respectively.

2.4.1. Whole-brain unpaired t-test

For the DWIs of PD patients and HCs, two datasets of DKI scalar measures were derived using the model fitting method and CNN method, respectively. FA maps were first registered to the MNI 152 standard space with resolution of 1mm isotropic using a combination of linear and non-linear transforms. The resulting transformation was then applied to all other DKI maps for co-registration. For DKI scalar measures of both methods, whole-brain unpaired t-tests were performed between PD patients and HCs to evaluate the ability of DKI to reveal the differences between the groups.

2.4.2. Tract-Based Spatial Statistics

Furthermore, we performed the Tract-Based Spatial Statistics (TBSS) analysis using the model fitting method and CNN method, respectively. TBSS extracted the mean FA maps to generate white matter skeleton, realized by a tool for nonparametric permutation inference implemented in FSL [28].

Threshold-Free Cluster Enhancement (TFCE) [29] based test was included in both whole-brain unpaired t-test and TBSS analysis to improve robustness compared with conventional voxel-based tests. All significance threshold was determined at $p < 0.05$ and corrected by family wise error (FWE).

It is noteworthy that we validated whether there were intra-group differences in HCs applying the analysis of whole-brain unpaired t-test and TBSS with model fitting method and CNN method respectively before comparing differences between the groups.

2.4.3. Correlation analysis

To determine the clinical significance of DKI scalar measures with CNN method more clearly, DKI scalar measures (MK, KFA, FA and MD) with model fitting or CNN method showing significant between-group differences in the basal ganglia (SN, putamen and caudate nucleus) were extracted and correlated with clinical assessments. Pearson's correlation analysis was used for normal distribution data and

Spearman's correlation was used for non-normal distribution data. Correlation with significance was defined at $p < 0.016$ (Bonferroni corrected). Statistical analyses were computed using IBM SPSS Statistics (version 25; IBM Corp., Armonk, NY) and GraphPad Prism 8.0.1.

3. Results

3.1. Demographic features

Age ($p = 0.659$, Student's t test) and sex distribution ($p = 0.092$, Pearson chi-square test) did not differ between PD and controls (Table 1).

3.2. The validation of intra-group difference in HCs

There were no significant differences of DKI scalar measures within healthy controls with model fitting and CNN methods.

3.3. Whole-brain unpaired t-test analysis

3.3.1. model fitting method

FA values in the bilateral anterior and superior corona radiata increased in PD patients compared to HCs. MD values in the caudate, putamen and thalamus bilaterally, and bilateral cerebral cortex and white matter, bilateral posterior thalamic radiation (include optic radiation), right sagittal stratum (including inferior longitudinal fasciculus and inferior fronto-occipital fasciculus), right cingulum (hippocampus), right superior and anterior corona radiata, and left fornix were significantly increased in PD patients compared with HCs. There was no significant difference of MK and KFA values between the groups (Figure. 3) ($p < 0.05$, FWE corrected).

3.3.2. CNN method

FA values increased in the bilateral superior corona radiata, left anterior corona radiata, left inferior fronto-occipital fasciculus and left uncinate fasciculus, while KFA values increased only in the left anterior corona radiata in PD patients compared to HCs. MD values in the left SN, left hippocampus, bilateral caudate nucleus and thalamus, bilateral cerebral cortex and white matter, bilateral anterior thalamic radiation, and forceps minor were obviously increased in PD patients compared with HCs. There was no significant difference of MK values between the groups (Fig. 3) ($p < 0.05$, FWE corrected).

3.4. TBSS analysis

3.4.1. model fitting method

MK values increased in the left anterior thalamic radiation, left inferior fronto-occipital fasciculus, left uncinate fasciculus, left inferior longitudinal fasciculus, left cingulum, left superior longitudinal fasciculus, left internal medullary lamina, and forceps minor in PD patients compared to HCs. FA values

were higher in the left superior corona radiata, left internal capsule (e.g., anterior thalamic radiation, corticospinal tract), left external capsule (e.g., inferior fronto-occipital fasciculus), left uncinate fasciculus, and left superior longitudinal fasciculus in PD patients compared to HCs. Compared with HCs, PD patients showed increased MD values in the bilateral inferior fronto-occipital fasciculus, bilateral inferior longitudinal fasciculus, bilateral uncinate fasciculus, bilateral anterior thalamic radiation, bilateral cingulum forceps major, and left superior longitudinal fasciculus. There was no significant difference of KFA value between the groups (Figure. 4). ($p < 0.05$, FWE corrected)

3.4.2. CNN method

MK values in the forceps minor, left inferior fronto-occipital fasciculus, left uncinate fasciculus, left cingulum, left anterior thalamic radiation increased significantly in PD patients. PD patients showed increased KFA and FA values in multiple brain regions, such as the bilateral anterior thalamic radiation, bilateral corticospinal tract and cingulum, bilateral inferior fronto-occipital fasciculus, bilateral inferior longitudinal fasciculus, bilateral superior longitudinal fasciculus, bilateral uncinate fasciculus, and forceps minor compared with HCs. We did not find a significant difference in MD values between the two groups (Figure. 4). ($p < 0.05$, FWE corrected)

3.5. Correlation analysis

3.5.1. model fitting method

We did not find any significant correlation between DKI scalar measures and clinical assessments in PD patients.

3.5.2. CNN method

We found positive correlation between the FA values of left putamen and H&Y scales ($r = 0.389$, $p = 0.001$). Negative correlation occurred between H&Y scales and FA and MK values in the right SN ($r=-0.390$, $p = 0.001$; and $r=-0.349$,$p = 0.004$, respectively) (Figure.5).

4. Discussion

The major finding of this study was that the CNN-estimated MD values in the left SN and bilateral caudate increased in PD patients compared to HCs. Additionally, the CNN-estimated FA and MK values in the right SN negatively correlated with H&Y scales and CNN-estimated FA values in the left putamen positively correlated with H&Y scales. In contrast, with model fitting method, there was no significant difference of MD values in the SN between PD patients and HCs, and there was no significant correlation between DKI scalar measures and clinical assessments in PD patients. Our findings suggest that the CNN method have the potential to optimize the estimation of DKI scalar measures and to improve the sensitivity to detect PD-related imaging features.

With CNN method, we found greater MD values in several brain regions in PD patients compared with HCs, especially in the left SN, which is consistent with previous reports using regions of interest (ROI)

analysis [10, 11, 14, 30–32]. PD is characterized by progressive death of dopaminergic neurons in the SN, followed by the loss of dopaminergic projections from the SN to striatum, resulting in a series of motor and non-motor symptoms [33]. According to the mathematical concept of tensor, the three-dimensional shape of diffusion elliptical structure depends on three eigenvalues (λ1, λ2, λ3) of orthogonal principal axes without directions. The MD value is the average of the three eigenvalues. The impaired axons and neurons and loss of myelin integrity in PD patients result in the decrease of restriction of water molecules displacement, which induces increased MD values [32, 34]. Regional increased MD values in the left SN and bilateral caudate estimated by CNN method are consistent with the pathological lesions in PD patients. In contrast, we did not find increased MD in the SN in PD patients compared to HCs by applying model fitting method. This finding indicates that CNN method can better reveal the pathological features of PD than model fitting method.

We did not observe modulation of FA and MK values in the SN in PD patients, which is in line with a previous report [14]. In contrast, some previous studies based on ROI analysis showed decreased or increased FA and/or increased MK in the SN in PD patients [6, 31]. We speculate that, first, different analysis methods may responsible for those controversial results. Whole-brain unpaired t-test, moving beyond the hypothesis-driven ROI analysis, focused the statistical information on each voxel accompanied with increased partial volume effects and false-positive risk, especially within the pathological brain tissues. Second, we suppose that these controversial findings may due to the heterogeneity of patients being recruited and variations imaging quality [3, 8]. In addition, it has been reported that iron deposition could increase FA values and decrease MD values in the white and gray matters [35]. Numerous reports have demonstrated that there was iron accumulation in the SN [36–38]. Thus, different levels of iron deposition in the SN may also be a reason contributing to these inconsistent findings.

We found negative correlation between H&Y scales and CNN-estimated FA values and MK values in the SN, as well as positive correlation between H&Y scales and CNN-estimated FA values in the putamen. These results indicate that FA and MK in the SN decreases, while FA in the putamen increases with the progression of the disease. As most of our patients were in the early stages (fifty-five of our patients were at H&Y stages 1 and 2), it is possible we could detect decreased FA in the SN if more advanced patients were enrolled. We did not find any significant correlation between DKI scalar measures and clinical assessments in PD patients using the model fitting method, which further proves that using CNN method to estimate DKI measures can improve the ability to explore PD-related neural modulations than using model fitting method.

For the TBSS analysis, increased FA values were observed in the brain white matter such as anterior thalamic radiation, inferior longitudinal fasciculus, superior longitudinal fasciculus, corticospinal tract, and inferior fronto-occipital fasciculus with both methods and agreed with previous studies [13, 39–41]. It has been shown that increased FA in these white matters correlated with better olfactory function and lower motor severity [42]. Thus, these increased diffusional properties of white matter might be a reflection of microstructural compensation [42].

We observed greater MK values in white matter in PD patients, which is inconsistent with previous reports. Previous studies found either no significant difference in MK values [43, 44], or decreased MK values of anterior cingulum, inferior fronto-occipital fasciculus and uncinate fasciculus in PD patients [7, 45]. We suppose that the heterogeneity of patients being recruited and differences in protocol of diffusion image acquisition and image processing may contribute to these inconsistent findings. In addition, we found increased KFA in white matter, which has not been reported previously. KFA values, resembling the FA definition, quantify the degree of anisotropy of the non-Gaussian diffusion. In the current study, the increased KFA and FA values are located in the same white matter fibers. So far, only a small number of studies have paid attention to the kurtosis changes of white matter in PD patients, it is necessary to perform large cohort studies to elucidate the microstructural changes in white matter in PD patients.

In conclusion, the CNN method has the potential to sensitively detect the nigral pathology and improve the robustness and performance of DKI images with few of DWIs and then to differentiate PD patents from HCs. In addition, compared with the model fitting method, CNN method can better find the relationship between DKI parameter measures and clinical assessments susceptibility. These findings approve that CNN can help to explore PD-associated imaging features.

List Of Abbreviations

CNN Convolutional neural network

DKI Diffusion kurtosis imaging

DTI Diffusion tensor imaging

DWI Diffusion-weighted image

FA Fractional anisotropy

FOV field of view

FSL FMRIB Software Library

FWE Family wise error

H&Y Hoehn & Yahr

HC healthy control

KFA Kurtosis fractional anisotropy

MD Mean diffusivity

MDS-UPDRS ШMovement Disorder Society Unified Parkinson’s Disease Rating Scale, part III

MK Mean kurtosis

MRI Magnetic resonance imaging

PD Parkinson’s disease

ROI Region of interest

SE-EPI Single shot spin-echo echo planar imaging sequences

SMS-EPI Simultaneous multi-slice diffusion echo planar imaging sequence

SN Substantia nigra

SNR Signal-to-noise ratio

TBSS Tract-based spatial statistics

TE Echo time

TFCE Threshold-Free Cluster Enhancement

TR Repetition time

Declarations

Availability of data and materials

The datasets used and/or analyzed during the current study are available from the corresponding author on reasonable request.

Competing interests

The authors declare that they have no competing interests

Funding

This research was supported by the Ministry of Science and Technology (2016YFC1306503), the National Science Foundation of China (82071423 and 8187142881571228), the Ministry of Science and Technology (2016YFC1306503), Beijing Municipal Commission of Health and Family Planning, No. PXM 2018_026283_000002, and the National Key Research and Development Program of China (2018YFC1312000), National Natural Science Foundation of China (81871428). The funding source had no involvement in study design, collection, analysis and interpretation of data, writing of the report, or in the decision to submit the article for publication.

Authors' contributions

Junyan Sun and Ruike Chen analyzed the data and wrote the manuscript. Qiqi Tong guided the analyses of diffusional MRI data. Tao Wu and Hongjian He designed and supervised the whole research and polished the manuscript. Jinghong Ma, Linlin Gao, and Dongling zhang collected clinical assessment of the recruited subjects. Jiliang Fang is responsible for the scanning and quality control of raw MRI data. Piu Chan polished the manuscript. All authors read and approved the final manuscript."

Acknowledgements

The authors sincerely thank the subjects for their cooperation.

References

1. Poewe W, Seppi K, Tanner CM (2017) Parkinson disease. Nat Rev Dis Primers 3:17013. doi:10.1038/nrdp.2017.13
2. Wong YC, Luk K, Purtell K (2019) Neuronal vulnerability in Parkinson disease: Should the focus be on axons and synaptic terminals? Mov Disord 34:1406–1422. doi:10.1002/mds.27823
3. Atkinson-Clement C, Pinto S, Eusebio A, Coulon O (2017) Diffusion tensor imaging in Parkinson's disease: Review and meta-analysis. Neuroimage Clin 16:98–110. doi:10.1016/j.nicl.2017.07.011
4. Cochrane CJ, Ebmeier KP (2013) Diffusion tensor imaging in parkinsonian syndromes: a systematic review and meta-analysis. Neurology 80:857–864. doi:10.1212/WNL.0b013e318284070c
5. Jensen JH, Helpern JA, Ramani A, Lu H, Kaczynski K (2005) Diffusional kurtosis imaging: the quantification of non-gaussian water diffusion by means of magnetic resonance imaging. Magn Reson Med 53:1432–1440
6. Wang JJ, Lin WY, Lu CS (2011) Parkinson disease: diagnostic utility of diffusion kurtosis imaging. Radiology 261:210–217. doi:10.1148/radiol.11102277
7. Kamagata K, Tomiyama H, Hatano T (2014) A preliminary diffusional kurtosis imaging study of Parkinson disease: comparison with conventional diffusion tensor imaging. Neuroradiology 56:251–258
8. Bergamino M, Keeling EG, Mishra VR, Stokes AM, Walsh RR (2020) Assessing White Matter Pathology in Early-Stage Parkinson Disease Using Diffusion MRI: A Systematic Review. Front Neurol 11:314. doi:10.3389/fneur.2020.00314
9. Vaillancourt DE, Spraker MB, Prodoehl J (2009) High-resolution diffusion tensor imaging in the substantia nigra of de novo Parkinson disease. Neurology 72:1378–1384. doi:10.1212/01.wnl.0000340982.01727.6e
10. Joshi N, Rolheiser TM, Fisk JD (2017) Lateralized microstructural changes in early-stage Parkinson's disease in anterior olfactory structures, but not in substantia nigra. J Neurol 264:1497–1505. doi:10.1007/s00415-017-8555-3
11. Loane C, Politis M, Kefalopoulou Z (2016) Aberrant nigral diffusion in Parkinson's disease: A longitudinal diffusion tensor imaging study. Mov Disord 31:1020–1026. doi:10.1002/mds.26606

12. Lenfeldt N, Larsson A, Nyberg L, Birgander R, Forsgren L (2015) Fractional anisotropy in the substantia nigra in Parkinson's disease: a complex picture. Eur J Neurol 22:1408–1414. doi:10.1111/ene.12760
13. Wen MC, Heng HSE, Lu Z (2018) Differential White Matter Regional Alterations in Motor Subtypes of Early Drug-Naive Parkinson's Disease Patients. Neurorehabil Neural Repair 32:129–141. doi:10.1177/1545968317753075
14. Schwarz ST, Abaei M, Gontu V, Morgan PS, Bajaj N, Auer DP (2013) Diffusion tensor imaging of nigral degeneration in Parkinson's disease: A region-of-interest and voxel-based study at 3 T and systematic review with meta-analysis. Neuroimage Clin 3:481–488. doi:10.1016/j.nicl.2013.10.006
15. Wang Q, Xu X, Zhang M (2010) Normal aging in the basal ganglia evaluated by eigenvalues of diffusion tensor imaging. AJNR Am J Neuroradiol 31:516–520. doi:10.3174/ajnr.A1862
16. Hansen B, Shemesh N, Jespersen SN (2016) Fast imaging of mean, axial and radial diffusion kurtosis. Neuroimage 142:381–393. doi:10.1016/j.neuroimage.2016.08.022
17. Liu M, Zhang J, Lian C, Shen D (2020) Weakly Supervised Deep Learning for Brain Disease Prognosis Using MRI and Incomplete Clinical Scores. IEEE Trans Cybern 50:3381–3392. doi:10.1109/tcyb.2019.2904186
18. Shamir RR, Duchin Y, Kim J (2019) Microelectrode Recordings Validate the Clinical Visualization of Subthalamic-Nucleus Based on 7T Magnetic Resonance Imaging and Machine Learning for Deep Brain Stimulation Surgery. Neurosurgery 84:749–757. doi:10.1093/neuros/nyy212
19. Zou L, Zheng J, Miao C, Mckeown MJ, Wang ZJ (2017) 3D CNN Based Automatic Diagnosis of Attention Deficit Hyperactivity Disorder Using Functional and Structural MRI. IEEE Access PP:1–1
20. Liu Z, Cao C, Ding S, Liu Z, Han T, Liu S (2018) Towards Clinical Diagnosis: Automated Stroke Lesion Segmentation on Multimodal MR Image Using Convolutional Neural Network. IEEE Access 6:57006–57016
21. Lin Y, Xue W, Hui S, Ling-Li Z, Dewen H (2018) Multi-center Brain Imaging Classification Using A Novel 3D CNN Approach. IEEE Access:1–1
22. Lecun Y, Boser B, Denker J (2014) Backpropagation Applied to Handwritten Zip Code Recognition. Neural Comput 1:541–551
23. Li Z, Gong T, Lin Z, He H, Zhong J (2019) Fast and Robust Diffusion Kurtosis Parametric Mapping Using a Three-dimensional Convolutional Neural Network. IEEE Access PP:1–1
24. Woolrich MW, Jbabdi S, Patenaude B (2009) Bayesian analysis of neuroimaging data in FSL. Neuroimage 45:S173–S186. doi:10.1016/j.neuroimage.2008.10.055
25. Tournier JD, Smith R, Raffelt D (2019) MRtrix3: A fast, flexible and open software framework for medical image processing and visualisation. Neuroimage 202. doi:10.1016/j.neuroimage.2019.116137
26. Andersson JLR, Sotiropoulos SN (2016) An integrated approach to correction for off-resonance effects and subject movement in diffusion MR imaging. Neuroimage 125:1063–1078. doi:10.1016/j.neuroimage.2015.10.019

27. Ades-Aron B, Veraart J, Kochunov P (2018) Evaluation of the accuracy and precision of the diffusion parameter EStImation with Gibbs and NoisE removal pipeline. Neuroimage 183:532–543. doi:10.1016/j.neuroimage.2018.07.066
28. Smith SM, Jenkinson M, Johansen-Berg H (2006) Tract-based spatial statistics: Voxelwise analysis of multi-subject diffusion data. Neuroimage 31:1487–1505. doi:10.1016/j.neuroimage.2006.02.024
29. Smith SM, Nichols TE (2009) Threshold-free cluster enhancement: Addressing problems of smoothing, threshold dependence and localisation in cluster inference. Neuroimage 44:83–98. doi:10.1016/j.neuroimage.2008.03.061
30. Du G, Lewis MM, Sen S (2012) Imaging nigral pathology and clinical progression in Parkinson's disease. Mov Disord 27:1636–1643. doi:10.1002/mds.25182
31. Zhang G, Zhang Y, Zhang C (2015) Diffusion Kurtosis Imaging of Substantia Nigra Is a Sensitive Method for Early Diagnosis and Disease Evaluation in Parkinson's Disease. Parkinsons Dis 2015:207624. doi:10.1155/2015/207624
32. Duncan GW, Firbank MJ, Yarnall AJ (2016) Gray and white matter imaging: A biomarker for cognitive impairment in early Parkinson's disease? Mov Disord 31:103–110. doi:10.1002/mds.26312
33. Braak H, Rüb U, Gai WP, Del Tredici K (2003) Idiopathic Parkinson's disease: possible routes by which vulnerable neuronal types may be subject to neuroinvasion by an unknown pathogen. J Neural Transm (Vienna) 110:517–536. doi:10.1007/s00702-002-0808-2
34. Concha L (2014) A macroscopic view of microstructure: using diffusion-weighted images to infer damage, repair, and plasticity of white matter. Neuroscience 276:14–28. doi:10.1016/j.neuroscience.2013.09.004
35. Xu X, Wang Q, Zhong J, Zhang M (2015) Iron deposition influences the measurement of water diffusion tensor in the human brain: a combined analysis of diffusion and iron-induced phase changes. Neuroradiology 57:1169–1178. doi:10.1007/s00234-015-1579-4
36. Martin WR, Wieler M, Gee M (2008) Midbrain iron content in early Parkinson disease: a potential biomarker of disease status. Neurology 70:1411–1417. doi:10.1212/01.wnl.0000286384.31050.b5
37. Ward RJ, Zucca FA, Duyn JH, Crichton RR, Zecca L (2014) The role of iron in brain ageing and neurodegenerative disorders. Lancet Neurol 13:1045–1060. doi:10.1016/s1474-4422(14)70117-6
38. Straub S, Schneider TM, Emmerich J (2017) Suitable reference tissues for quantitative susceptibility mapping of the brain. Magn Reson Med 78:204–214. doi:10.1002/mrm.26369
39. Chen NK, Chou YH, Sundman M (2018) Alteration of Diffusion-Tensor Magnetic Resonance Imaging Measures in Brain Regions Involved in Early Stages of Parkinson's Disease. Brain Connect 8:343–349. doi:10.1089/brain.2017.0558
40. Taylor KI, Sambataro F, Boess F, Bertolino A, Dukart J (2018) Progressive Decline in Gray and White Matter Integrity in de novo Parkinson's Disease: An Analysis of Longitudinal Parkinson Progression Markers Initiative Diffusion Tensor Imaging Data. Front Aging Neurosci 10:318. doi:10.3389/fnagi.2018.00318

41. Wen MC, Heng HS, Ng SY, Tan LC, Chan LL, Tan EK (2016) White matter microstructural characteristics in newly diagnosed Parkinson's disease: An unbiased whole-brain study. Sci Rep 6:35601. doi:10.1038/srep35601
42. Sanjari Moghaddam H, Dolatshahi M, Mohebi F, Aarabi MH (2020) Structural white matter alterations as compensatory mechanisms in Parkinson's disease: A systematic review of diffusion tensor imaging studies. J Neurosci Res 98:1398–1416. doi:10.1002/jnr.24617
43. Surova Y, Nilsson M, Lampinen B (2018) Alteration of putaminal fractional anisotropy in Parkinson's disease: a longitudinal diffusion kurtosis imaging study. Neuroradiology 60:247–254. doi:10.1007/s00234-017-1971-3
44. Surova Y, Lampinen B, Nilsson M (2016) Alterations of Diffusion Kurtosis and Neurite Density Measures in Deep Grey Matter and White Matter in Parkinson's Disease. PLoS One 11:e0157755. doi:10.1371/journal.pone.0157755
45. Kamagata K, Tomiyama H, Motoi Y (2013) Diffusional kurtosis imaging of cingulate fibers in Parkinson disease: comparison with conventional diffusion tensor imaging. Magn Reson Imaging 31:1501–1506. doi:10.1016/j.mri.2013.06.009

Figures

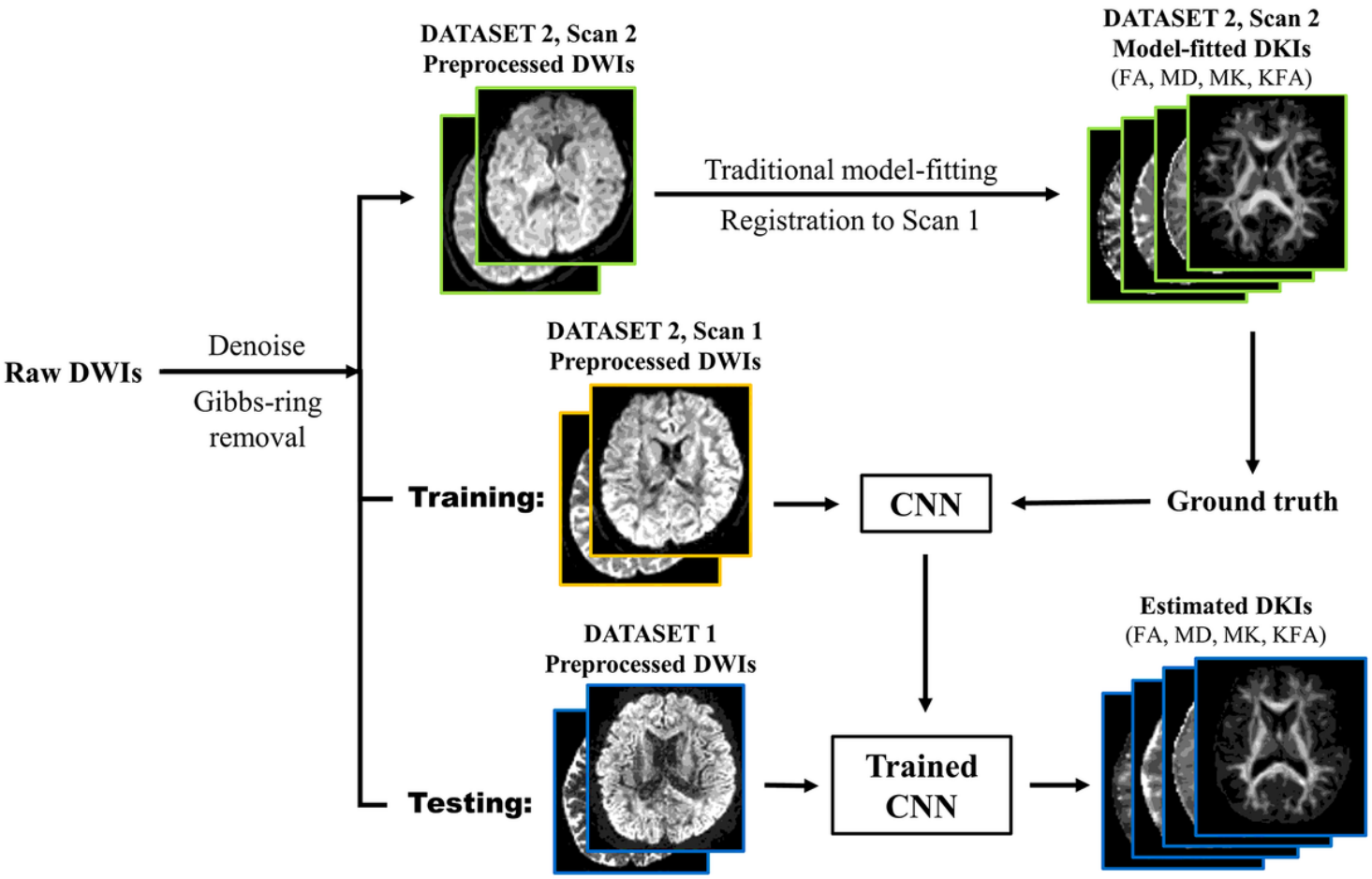

Figure 1

The training and testing pipeline of CNN method. Note. CNN=convolutional neural network; DWI=diffusion weighted image; DKI=diffusion kurtosis imaging; FA=fractional anisotropy; MD=mean diffusivity; MK=mean kurtosis; KFA=kurtosis fractional anisotropy.

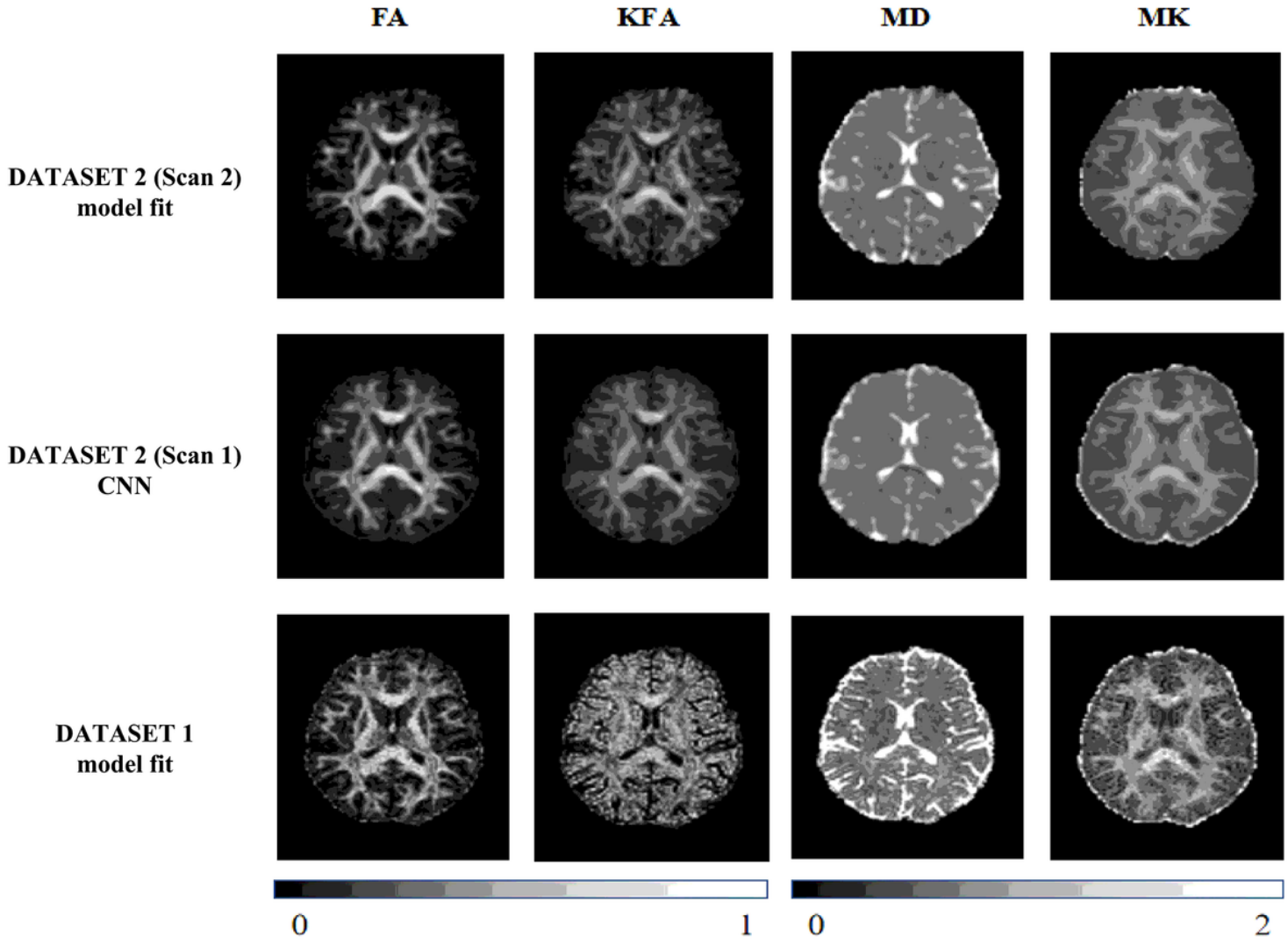

Figure 2

Maps of DKI scalar measures of subjects with different methods. Note. the high quality of DKI scalar maps with model fitting method in first line; the moderate quality of DKI scalar maps with model fitting method in last line; the moderate quality of DKI scalar maps with CNN method in middle line, indicating that the CNN method can optimize the scalar maps of moderate DWIs.

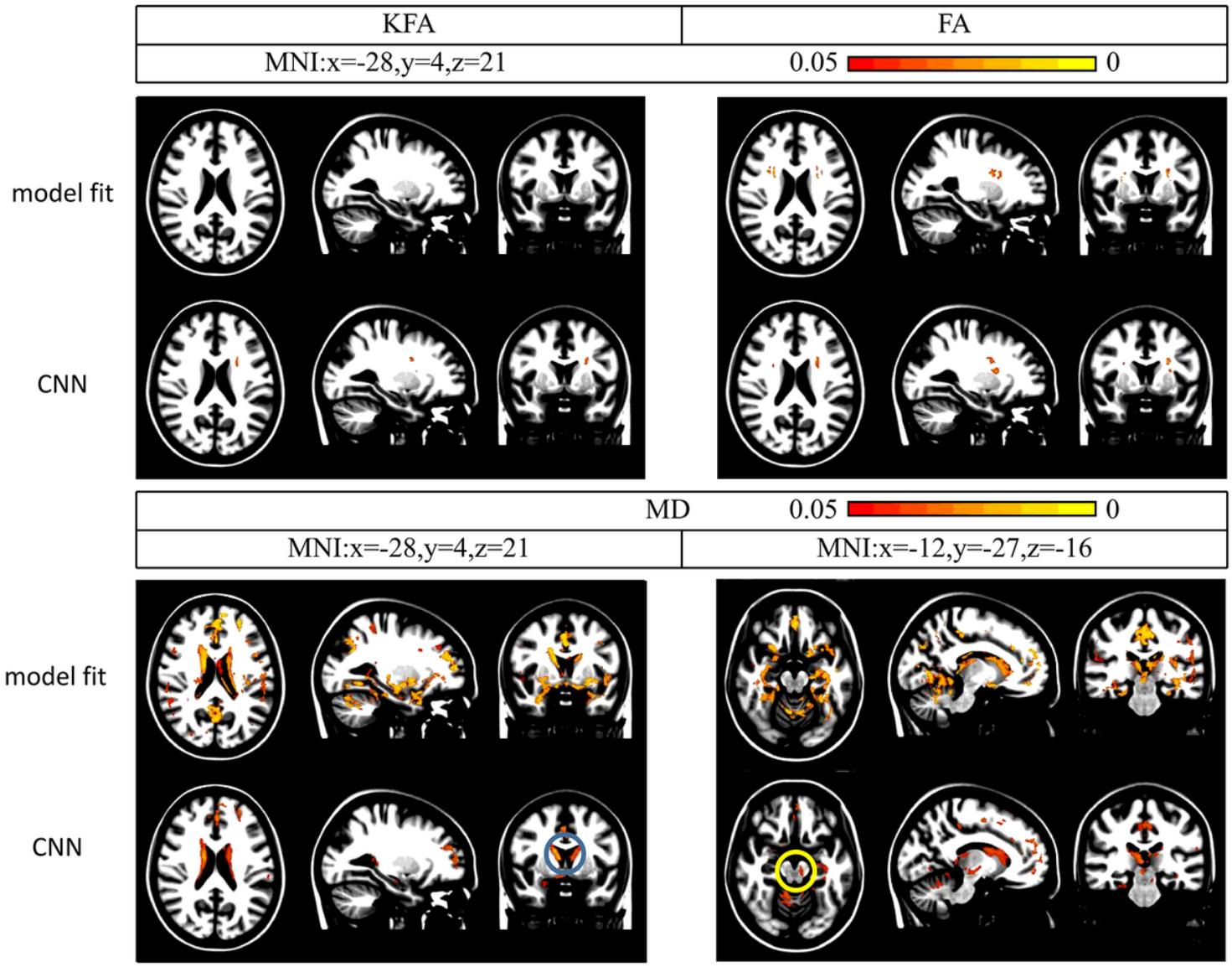

Figure 3

The whole-brain unpaired t-test analysis of DKI measures with CNN and model fitting methods. Note. Increased MD values in bilateral caudate (blue circle) and right SN (yellow circle) with the CNN method between HC and PD groups ($p < 0.05$, corrected by family wise error). KFA=kurtosis fractional anisotropy; FA=fractional anisotropy; MD=mean diffusivity; CNN= convolutional neural network; HC=healthy controls; PD, Parkinson's disease; MNI=Montreal Neurological Institute coordinate.

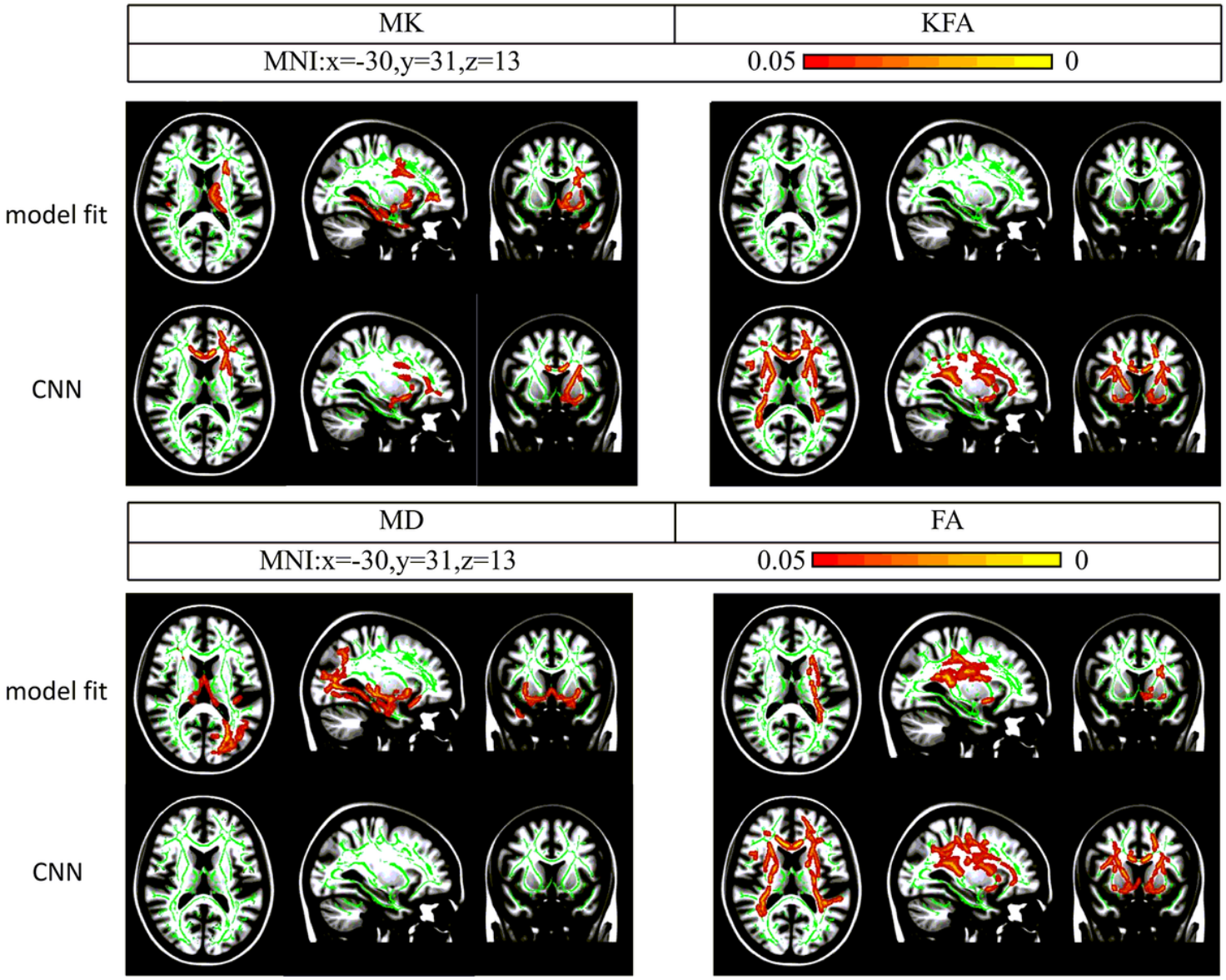

Figure 4

The TBSS analysis of DKI measures with CNN and model fitting methods. MK=mean kurtosis.

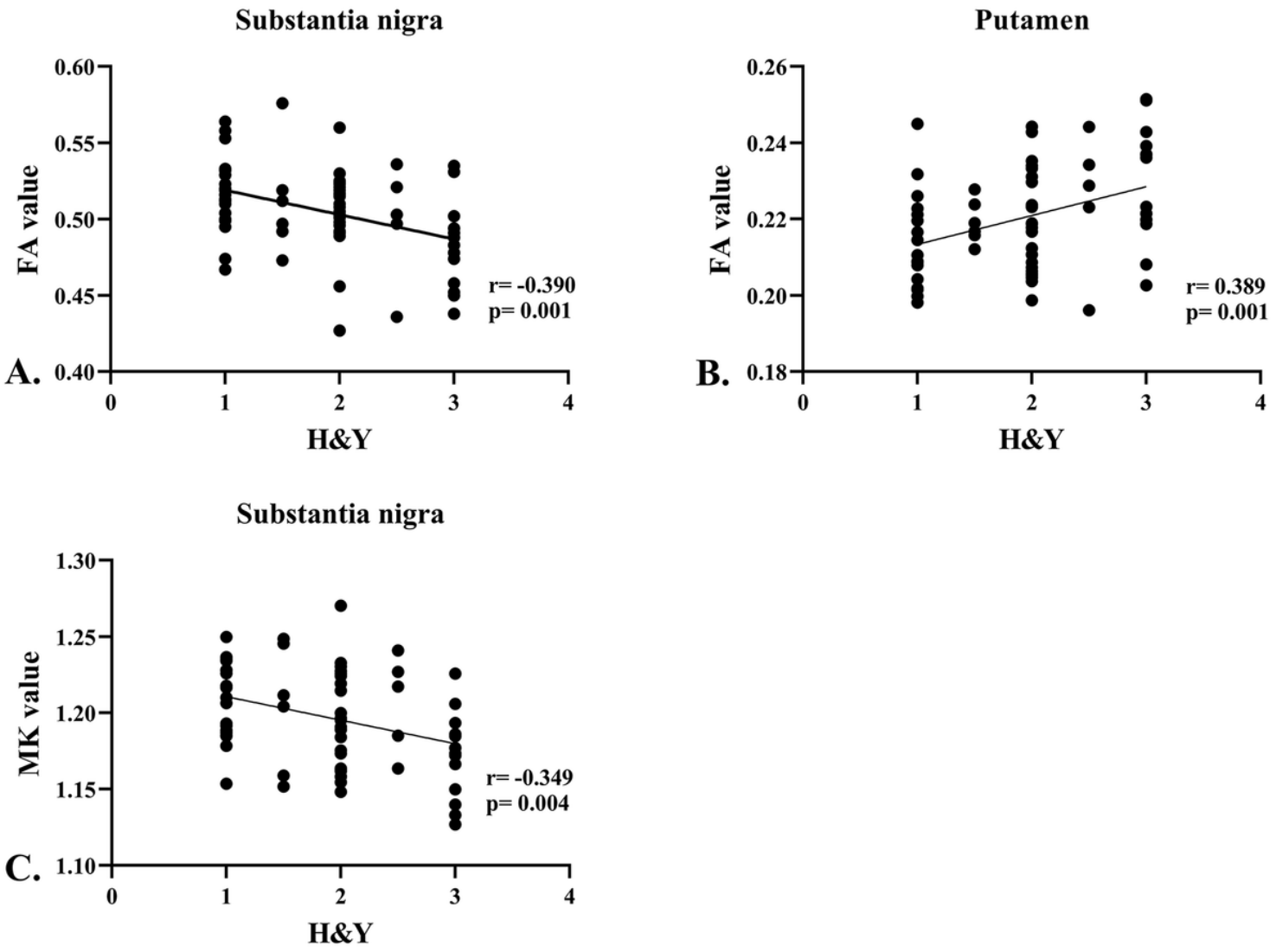

Figure 5

Spearman's correlation between the DKI scalar measures and H&Y scales. A. the negative correlation between the FA values of substantia nigra and H&Y scales; B. the positive correlation between the FA values of putamen and H&Y scales; C. the negative correlation between the MK values of substantia nigra and H&Y scales; H&Y scales=Hoehn & Yahr scales